Analysis of Magnetospheric Electron Data From PET

SRL technical report #94-1

Richard Selesnick

July 28, 1994

This report is a follow up to SRL technical report 93-1 in which I described the results of the PET electron calibrations and some preliminary data analysis. Here I describe a much more detailed attempt to understand the magnetospheric electrons observations using the calibration results. The primary difficulty in analyzing the PET data is the inability to determine the local pitch-angles of the measured electrons, due to the wide angular response of PET, especially for the P1 detector (see SRL technical report 93-1). Additional difficulties result from the high counting rates that occur in the magnetosphere which cause pulse pileup and chance coincidences. Because of the chance coincidence problem, the ELO type events are of limited value. In this report I have restricted the data to P1 singles rates and events from the time period when PET was commanded to accept P1 singles events in the ELO event type.

Although it is not possible to determine the electron pitch-angle distribution from a single point measurement, it is possible by combining data from an extended time period if certain assumptions are made. The approach that I have taken is as follows. I take a complete day of data and divide it into L shell intervals each of which will be analyzed independently. For each interval I calculate an average energy spectrum from the event data assuming an isotropic electron distribution. Then, using the derived energy spectrum, I fit a model pitch-angle distribution to the rate data assuming that the there are no time variations during the day. Although time variations will certainly occur, their significance can be inferred from the quality of the fit, and the result of the fit should be a reasonable daily average.

The energy spectra are calculated in the same way as described in SRL technical report 93-1, so I do not repeat that here. However, some care must be taken to minimize the effects of pileup in the high rate regions. The spectral fits and problems introduced by pileup are illustrated in Figures 1 and 2. They show P1 pulse height spectra from 1993 day 315 in six L shell intervals between 3 and 6. Model fits to the data are based on an exponential energy spectrum, $j = A \exp(-E/E_0)$, where A and E_0 are fit parameters. In Figure 1 the data were selected only from times where the P1 rate (not corrected for deadtime) was less than 10^4 s^{-1} and Figure 2 shows similar plots but only from times where the P1 rate was less than 2×10^4 s^{-1}. Between L values of 3.5 and 5.5 where the electron fluxes are high there is a dramatic hardening of the spectra from Figure 1 to Figure 2. The e-folding energies change from values near 0.4 MeV in Figure 1 to values near 4 MeV in Figure 2, although the fits are not very good in Figure 2. While it is possible that the spectra could harden when the flux increases, it seems unlikely that there could be such dramatic change. I interpret the hardening as a result of pileup of low energy electrons. Near the P1 threshold. This would, at least qualitatively, produce the effect shown. It would be possible to model the pileup based on the P1 calibration and the amplifier characteristics and this work was started by Dick Mewaldt in his 11/23/93 memo, but it is a substantial effort. Instead, I have chosen to simply restrict the spectra to P1 rates less than 10^4 s^{-1} as in Figure 1 and assume that they do not vary with intensity or time during the day.

Once the energy spectra are determined, the P1 rates, which have good time resolution, can be used to determine the pitch-angle distribution. This is because the SAMPEX orbit goes through different magnetic field values on a given L shell. The variation in flux with field magnitude B is related to the variation with pitch-angle α by the conservation of the magnetic moment according to

$$\frac{\sin^2\alpha}{B} = \frac{\sin^2\alpha_0}{B_0} \tag{1}$$

where the subscript 0 refers to equatorial values.

To simplify the procedure, I use the rate data by averaging all quantities over each individual time period during which SAMPEX is in the L shell ranges shown in Figure 1. This produces 4 rate values per orbit and ~60 per day for each L interval. Associated with each rate value are values of B/B_0, the angle θ_B of the PET axis relative to the magnetic field, and the equatorial atmospheric bounce loss-cone angle α_{0b} defined by

$$\sin^2\alpha_{0b} = \frac{B_0}{B_{100}} \tag{2}$$

where B_{100} is the minimum of the two field magnitudes at 100 km altitude on the same field line in either hemisphere.

The values of α_{0b} from 1993 day 280 are shown in Figure 3 for each L shell interval. They are plotted verses longitude in the offset-tilted-dipole (OTD), or eccentric dipole, coordinate system. This removes the effect of the Earth's dipole tilt, so that the longitudes of a given field line in the northern and southern hemispheres are nearly equal. Since α_{0b} is a property of the field model, the shapes of the curves in Figure 3 do not vary from day to day, although the longitudes of the data points do. The variation of α_{0b} with OTD longitude is, roughly speaking, a result of the dipole offset. It leads to the drift loss cone, which has a constant equatorial angle α_{0d} equal to the maximum value of α_{0b} for a given L range. Electrons with α_0 less than α_{0b} will be lost to the atmosphere (or mirror below 100 km) on the next bounce. Electrons with α_0 greater than α_{0b} but less than α_{0d} will remain trapped only until their drift motion takes them to a longitude where α_0 becomes equal to α_{0b} and then they will be lost. These quasi-trapped electrons are in the drift loss cone. Electrons with α_0 greater than α_{0d} will remain trapped indefinitely, or until they are scattered into the loss-cone. These are stably trapped electrons.

When α_{0b} is converted to the local bounce loss-cone angle α_b using (1) typical values for the SAMPEX orbit are near 60°, while the local drift loss-cone angle α_d is usually at 90° (i.e. stably trapped particles do not have access). However, near the peak α_{0b} values, at ~70° OTD longitude, the northern α_b values are at 90° so that only precipitating electrons have access, while the southern α_d values are less than 90° allowing access to stably trapped electrons. The locations of the three regions, where only precipitating particles have access, where precipitating and quasi-trapped particles have access, and where precipitating, quasi-trapped and stably-trapped particles have access, are indicated in Figure 3 and in successive figures by different symbol types. Note that 0° OTD longitude is defined by the plane of the dipole and Earth's rotation axis so that 70° OTD longitude is near 0° geographic longitude. The maximum in α_{0b} near 70° OTD longitude is caused by the south Atlantic anomaly (SAA), while the secondary maximum near 250° OTD longitude is caused by the lesser known north Pacific anomaly.

The particle access issues described above are important for determining the PET counting rates, because one would expect the trapped particle fluxes to normally be higher than the loss-cone fluxes. To determine this I have chosen a simple model electron intensity to fit to the rate data:

$$j(E,\alpha) = \begin{cases} C_1 e^{-E/E_0}, & \alpha < \alpha_b \\ C_2 \left[\dfrac{\phi-\phi_0}{2\pi}\right] e^{-E/E_0} \left[\dfrac{B_0}{B}\right]^n \sin^{2n}\alpha, & \alpha_b < \alpha < \alpha_d \\ C_3 e^{-E/E_0} \left[\dfrac{B_0}{B}\right]^n \sin^{2n}\alpha, & \alpha_d < \alpha < \dfrac{\pi}{2} \end{cases} \tag{3}$$

where ϕ is the OTD longitude in radians and ϕ_0 is the OTD longitude of the maximum α_{0b} value. There are four fit parameters: C_1, C_2, C_3, and n. The intensity in the drift loss-cone ($\alpha_b < \alpha < \alpha_d$) is assumed to increase linearly with ϕ after being depleted in the SAA due to a constant rate of pitch angle diffusion into the loss-cone, which also explains the uniform intensity in the bounce loss-cone.

Given the model intensity defined above, the P1 counting rate is

$$r = \int_0^{2\pi}\int_0^{\pi}\int_0^{\infty} R(E,\theta)\; j(E,\alpha(\theta,\phi))\; dE\; \sin\theta\; d\theta\; d\phi \tag{4}$$

where θ and ϕ are spherical angles relative to the telescope axis, and $R(E,\theta)$ is the P1 response function. The model intensity is converted from a function of α to one of θ and ϕ by

$$\sin^2\alpha = \sin^2\theta[\sin^2\phi + (\cos\phi\cos\theta_B - \cot\theta\sin\theta_B)^2] \tag{5}$$

The triple integral in (4) must then be done numerically. However, since (4) must be evaluated many times to determine the rates for different values of the fit parameters in (3), it would be extremely slow have to evaluate the integrals each time. I have formed a look-up table for the integral at various values of the parameters and use linear interpolation for intermediate values. The table is a function of four variables: E_0, n, θ_B, and α_i which is either of the two loss-cone angles. The integrals for the table are done with α varying from α_i to $\pi/2$. The bounce loss-cone integral is then evaluated as the difference of two table entries with $n = 0$, the drift loss-cone integral is the difference of two entries with $n \neq 0$, and the stably-trapped integral is a single entry with $n \neq 0$. The complete integral in (4) is then the sum of these three.

The model parameters are varied until (4) gives a best fit between the predicted and observed P1 rates for a given day and L shell interval. However, there is often a fair amount of scatter in the data points, with a few outliers that can have an undue influence on a simple least-squares fit. It is therefore necessary to use a more robust fitting technique. The least-squares technique assumes a Gaussian probability distribution for the errors in the data points. If instead one assumes a Cauchy (or Lorentzian) distribution, which is also bell-shaped but has much more probability in the tails of the distribution, then the outliers are essentially ignored and the fit converges to a model that is close to most of the data points (see e.g. Press et al., Numerical Recipes, p. 542). In this case one minimizes the sum of $\log(1+z_i^2/2)$ for each data point i, where $z_i=(y_i-\tilde{y}_i)/\sigma_i$, y_i is the ith data point with uncertainty σ_i, and $\tilde{y}_i$ is the model data point. For y_i I have used the natural logarithm of the counting rates with $\sigma_i = 0.2$. The minimization is done using the Numerical Recipes simplex algorithm AMOEBA.

As a first example of a model fit, the P1 data and model counting rates from 1993 day 270 are shown in Figure 4, with a similar format to Figure 3. The three regions of the model are clearly visible in each L range. The bounce-loss region is the group of low counting rates with ϕ *wig* < 100°. The drift-loss cone region is the group of intermediate counting rates with $\phi \gtrsim 100°$ that are slowly increasing with ϕ due to the filling of the drift loss-cone. The stably-trapped region is the group of high counting rates with ϕ *wig* < 100°. Also seen are several outlier points, especially at low counting rates in the drift loss-cone region and at low L values. In this case there is a clear separation between

the intensity levels in the three regions. Considering the simplicity of the model, the quality of the fit is perhaps surprisingly good, although there is considerably more scatter in the data points than in the model predictions. I discuss this a little more later.

A second fit example is shown in Figure 5 for 1993 day 315. Here most of the counting rates are considerably higher than in the previous example, approaching values of 10^5 s^{-1}. At these high rates the deadtime corrections cannot be trusted, as can be seen from the saturation effects in the high intensity regions. However, where the counting rates are low, in the bounce loss-cone regions and at the high and low L shells, the model should still give reasonable results. The best way to decide whether the rates are too high is by inspection of these type of plots. I think that it is impractical to place an upper limit on the rates because the scatter in the data points would then tend to bias the model to low intensity. However, a criterion based on the average rate in a given region could probably be used safely.

One reason for the higher counting rates in Figure 5 relative to Figure 4 is the difference in the pointing directions of PET due to the 3 month periodicity of the orbit. During 1993 day 270 PET is consistently pointing nearly parallel or anti-parallel to the magnetic field, but during 1993 day 315, 45 days later, it often points nearly perpendicular to the magnetic field, as shown in Figure 6. Because of the wide loss-cone angles at the SAMPEX orbit, the trapped and quasi-trapped electrons are moving nearly perpendicular to the field. The PET response function at large angles to the telescope axis is substantially reduced relative to that for small angles, leading to lower rates. The rates from the high intensity regions are therefore most valid when θ_B is not near 90° because saturation effects are reduced. However, the response functions at high incidence angles are also less accurate than at lower angles due to the nature of the calibrations.

The saturation effects in Figure 5 are also evident by the small differences in the observed rates for different θB values, compared to the large differences in the model predictions. This is clearly apparent for the stably-trapped population where the anisotropy is largest. At the low and high L shells, where the intensities are lower, the data match the model predictions more closely, indicating that saturation is less significant. One possibility is to throw out the data when θ_B is near 90°. This results in the fit shown if Figure 7. Here the model intensities in the intermediate L shells are considerably higher because saturation is less significant, but it clearly still occurs at the highest counting rates. In the following analysis I do not place any restrictions on θ_B, although such a scheme probably would be useful. However, when the rates are not too high, the occurrence of varying θ_B values provides particularly strong constraints on the model parameters.

Once the model parameters have been determined, the electron intensity can be determined at any point along the field line by using Liouville's theorem, which says that $j(E,\alpha) = j_0(E,\alpha 0)$, and the scaling given by (1). Of course, this is only valid to the extent that the the model intensity (4) represents the true intensity. The results of a preliminary set of model fits for 23 days are shown in Figure 8. Here the omnidirectional, integral intensity has been evaluated at the SAMPEX location and averaged over ϕ for each of the three model regions. The stably-trapped electron intensities appear to be lower than the quasi-trapped values because they are seen only over a limited ϕ interval, while the average is over all ϕ.

The first group of days in Figure 8 is during the period when PET is pointing primarily along the magnetic field, and the results from this period should be valid. For the second group of days PET is pointing closer to perpendicular to the field. By inspection of the fits as in Figure 5, it is evident that there are some saturation effects in the stably-trapped population throughout this period. At day 309 there is a substantial increase in the precipitating intensity which is real because the counting rates are still relatively low, but is not reflected by similar increases in the quasi-trapped and stably-trapped intensities. These are strongly effected by saturation and represent only lower limits on the true values. As an illustration of this period of elevated intensities the model fit from 1993 day 313 in shown in Figure 9.

In summary, the P1 rates can be used to estimate the intensities of each of the three electron populations, except when the rates are too high for accurate deadtime corrections and care must be taken to identify these periods. Similar calculations could be done with the ELO data, but then additional difficulties would be introduced by chance coincidences. However, if one is interested only in the precipitating intensity, where the rates are low, then the chance coincidence problem may not be too bad. The fits to the P1 rates are generally fairly good, although there is typically more scatter in the rate data than the in model predictions. This is probably due to a combination of time variations during the day and innaccuracies in the intensity model, but there also appear to be some systematic effects that are not organized by OTD longitude and reappear over several successive days. These may be due to innacuracies in the determination of drift shells by the magnetic field model. Finally, there are certainly possibilities for improving the analysis depending on the desired application. For example, the definition of the bounce loss-cone angle using the 100 km point is somewhat arbitrary, and there is clearly some organized structure in the precipiting intensities that is not accounted for by the simple model of a uniform intensity in the loss cone. More detailed models could probably be devloped to account for this structure.

Figure Captions

1. Event data (histograms) from P1 during 1993 day 315 for different L shell ranges. The data were restricted to time periods when the P1 uncorrected rate was less than 10^4 s^{-1}. The x-symbols show simulations of the data based on least-squares fits of an isotropic, exponential intensity model.

2. Similar to Figure 1 but the event data were restricted to time periods when the P1 uncorrected rate was less than 2×10^4 s^{-1}.

3. Equatorial bounce loss-cone angles versus offset-tilted-dipole (OTD) longitude for 1993 day 280. Each point is an average over a single SAMPEX pass through the indicated L shell range. Symbols with four (three) vertices indicate that SAMPEX was in the northern (southern) hemisphere. Solid symbols (filled squares or triangles) are in regions where the local bounce loss-cone angle at SAMPEX is less than 90° but the local drift loss-cone angle is 90°. Open triangles are in regions where the local drift loss-cone angle is less than 90° (these occurr only in the southern hemisphere). Four-cornered stars are in regions where the local bounce loss-cone angle is 90° (these occurr only in the northern hemisphere). The same symbol conventions are used in the following figures.

4. Counting rates from 1993 day 270. The data are represented by the skeletal symbols (center connected to vertices) with four (three) vertices for the northern (southern) hemisphere. The model fit to the data is represented by the symbol types defined in Figure 3.

5. Similar to Figure 4 but for 1993 day 315.

6. The angles of the PET axis from the local magnetic field for 1993 day 315.

7. Similar to Figure 5 but excluding data points with $60° < \theta_B < 90°$.

8a and 8b. Average omnidirectional intensities from the model fits (0.5 to 2.5 MeV) for the precipitating (stars), quasi-trapped (filled squares), and stably trapped (open squares) electron populations, as seen at SAMPEX.

9. Similar to Figure 4 but for 1993 day 313.

93/315 2 < 10000 <

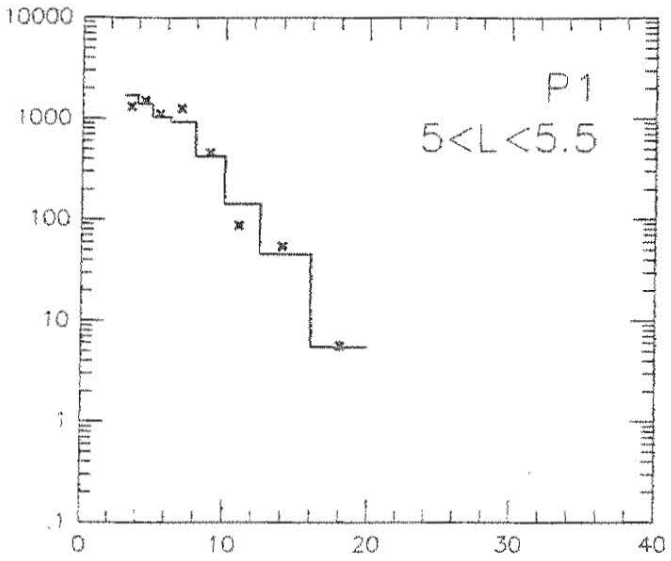

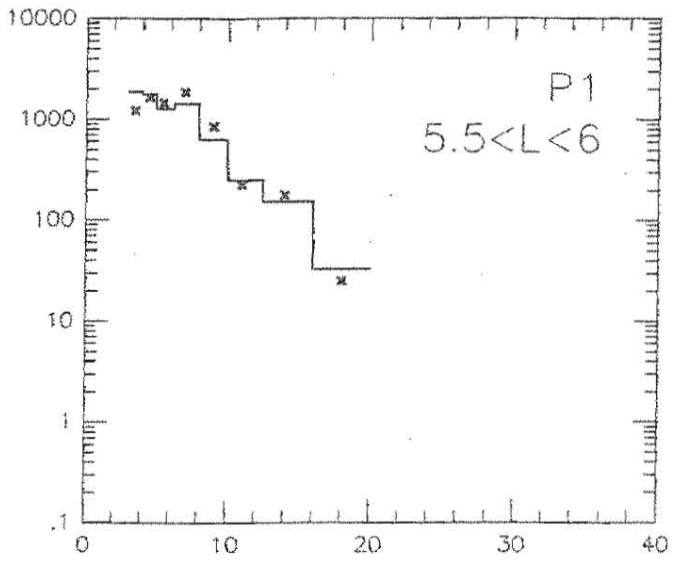

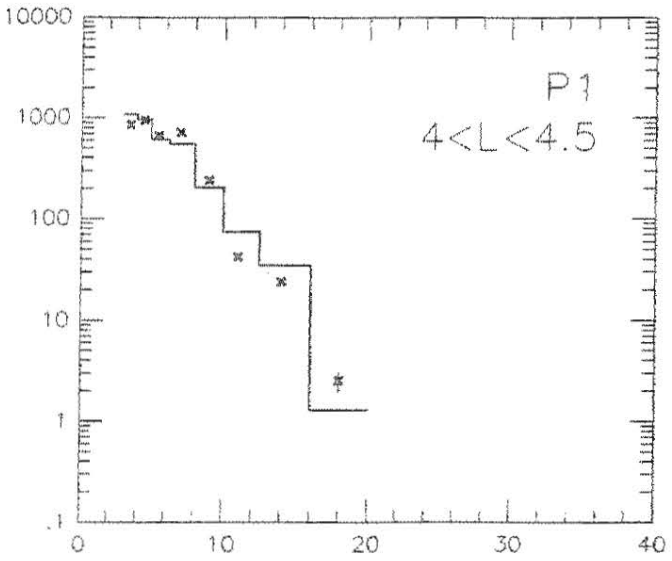

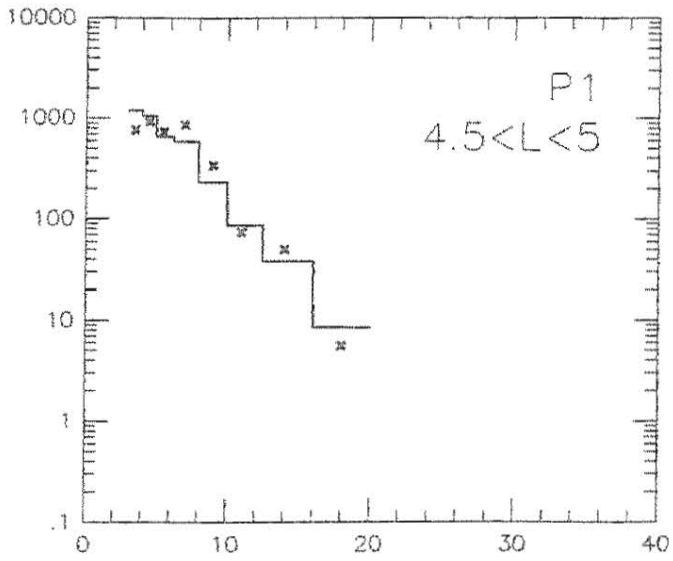

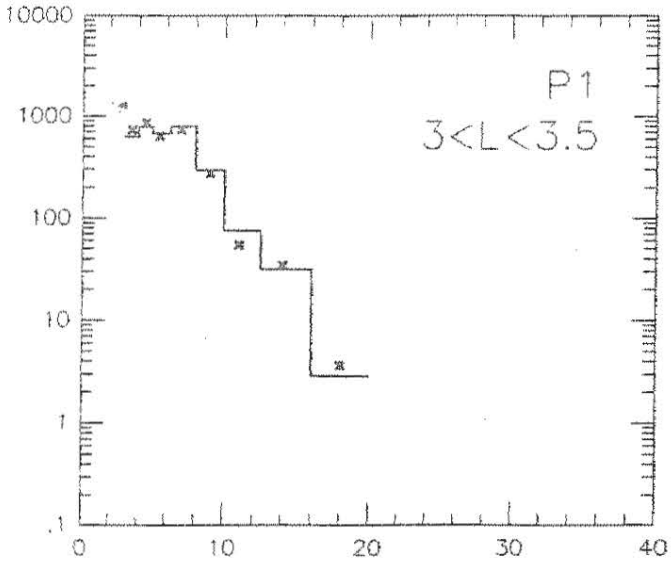

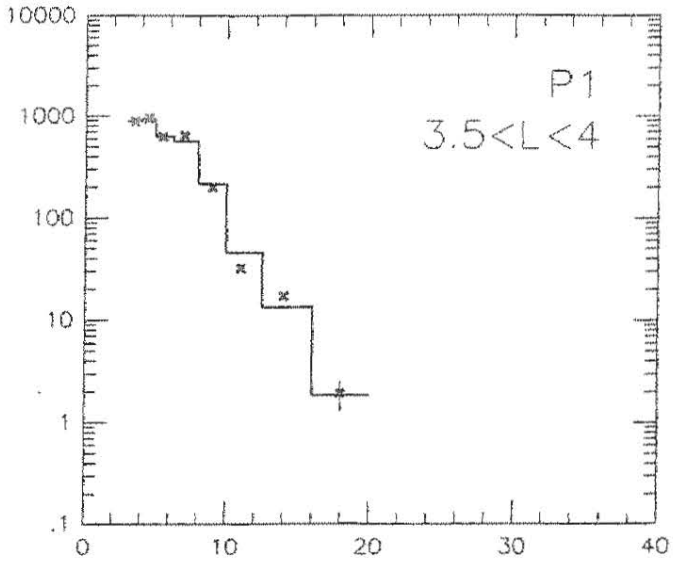

93/3:5 P1 < 2.5?? 5

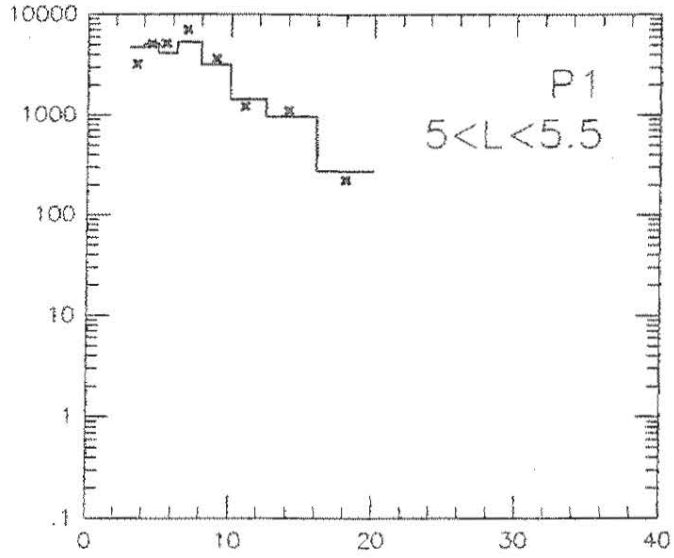
P1
5<L<5.5
10000
1000
100
10
1
.1
0
10
20
30
40

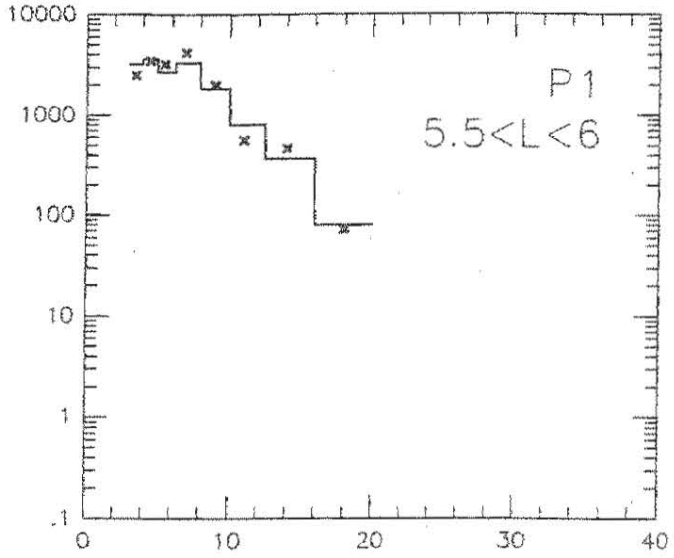
P1
5.5<L<6
10000
1000
100
10
1
.1
0
10
20
30
40

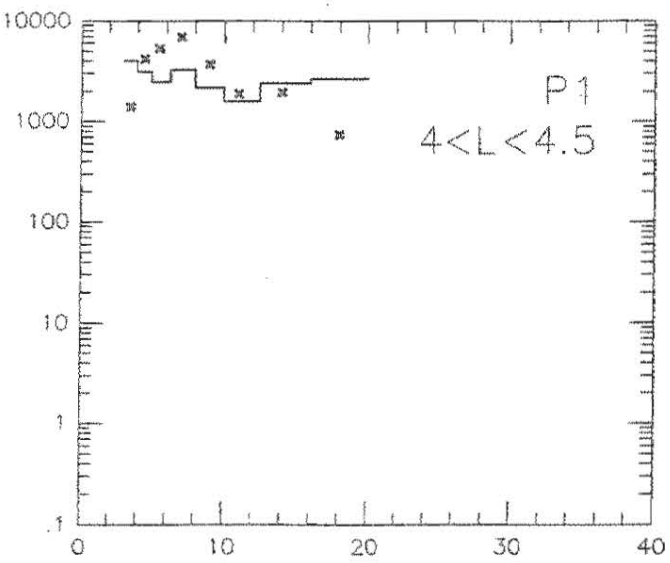
P1
4<L<4.5
10000
1000
100
10
1
.1
0
10
20
30
40

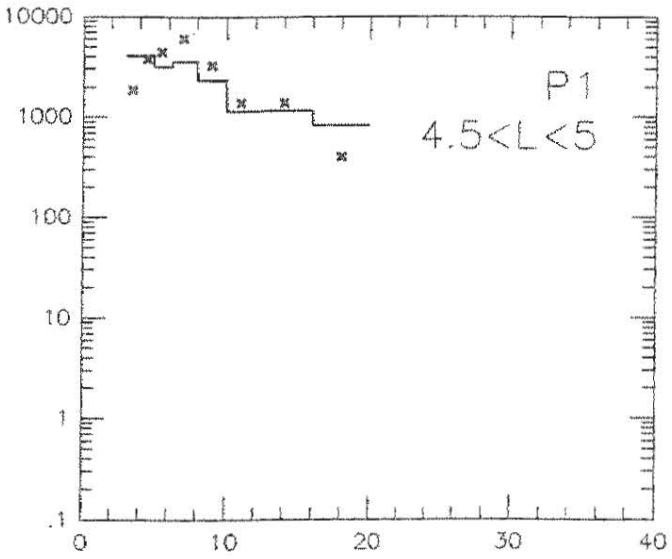
P1
4.5<L<5
10000
1000
100
10
1
.1
0
10
20
30
40

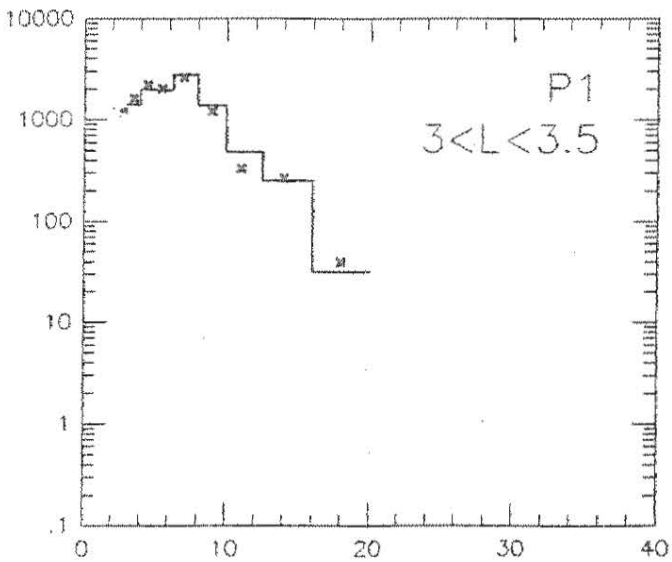
P1
3<L<3.5
10000
1000
100
10
1
.1
0
10
20
30
40

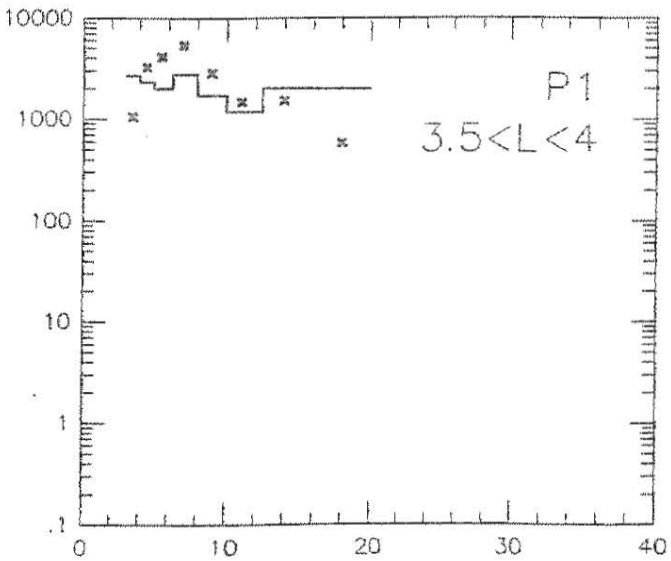
P1
3.5<L<4
10000
1000
100
10
1
.1
0
10
20
30
40

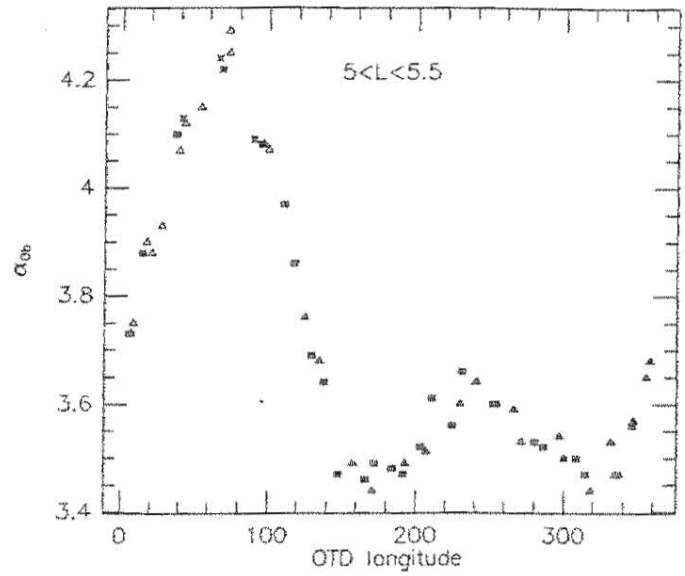
5<L<5.5
α_{Ob}
OTD longitude

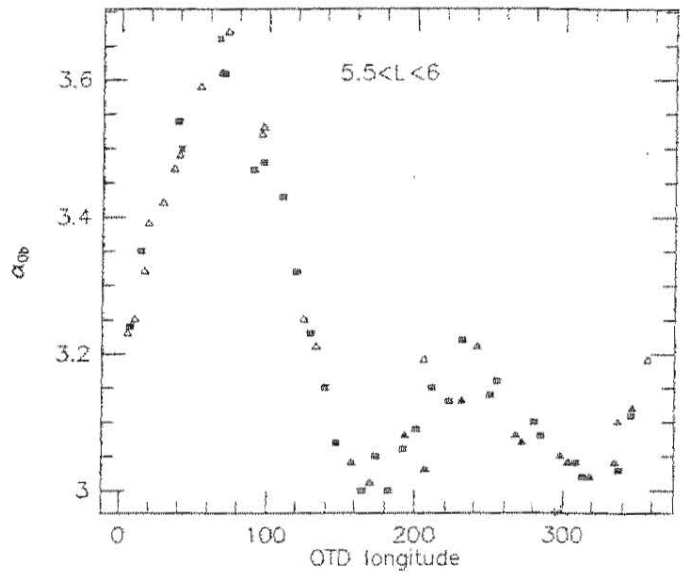
5.5<L<6
α_{Ob}
OTD longitude

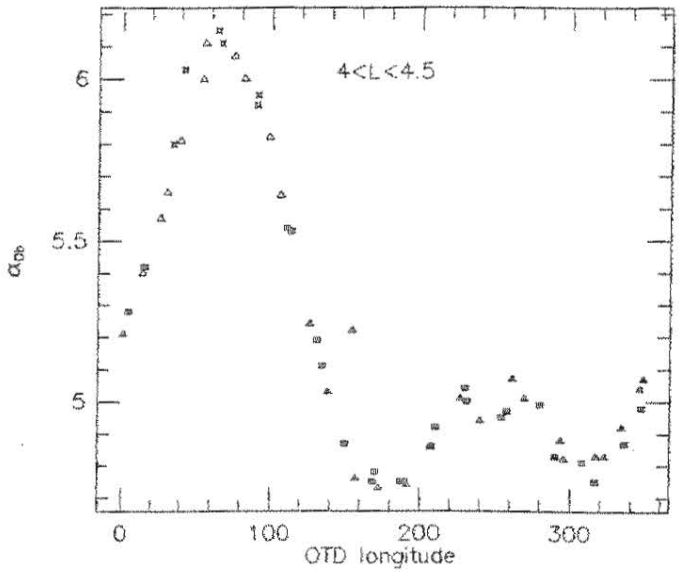
4<L<4.5
α_{Ob}
OTD longitude

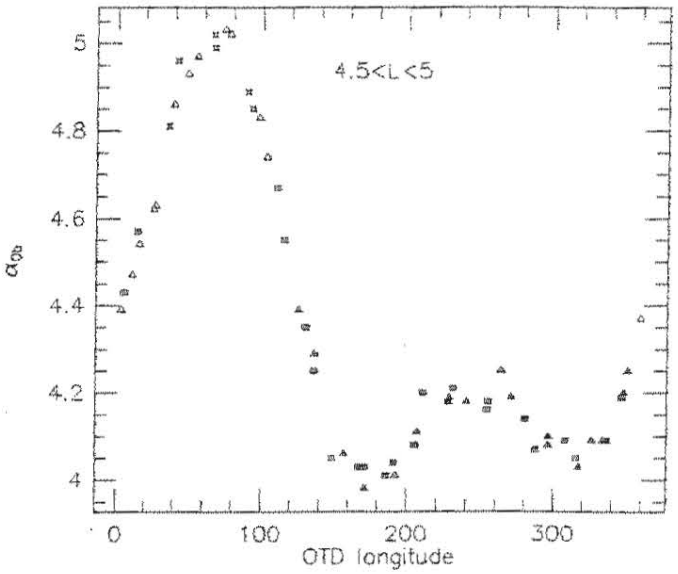
4.5<L<5
α_{Ob}
OTD longitude

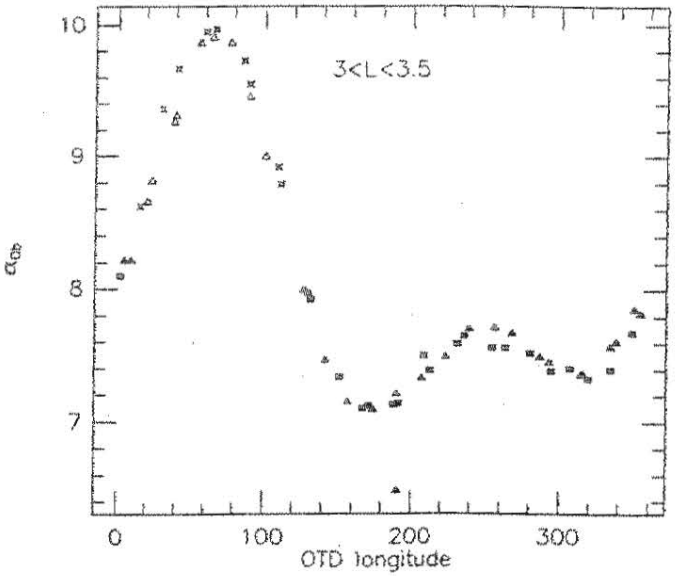
3<L<3.5
α_{Ob}
OTD longitude

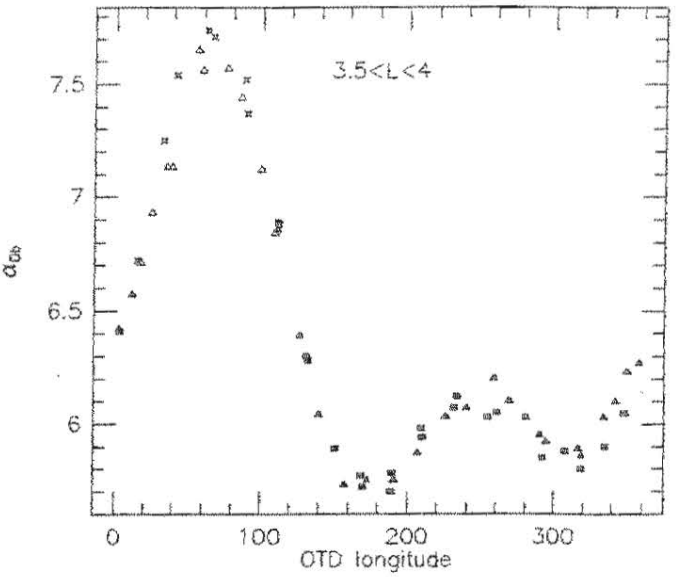
3.5<L<4
α_{Ob}
OTD longitude

93/27/8

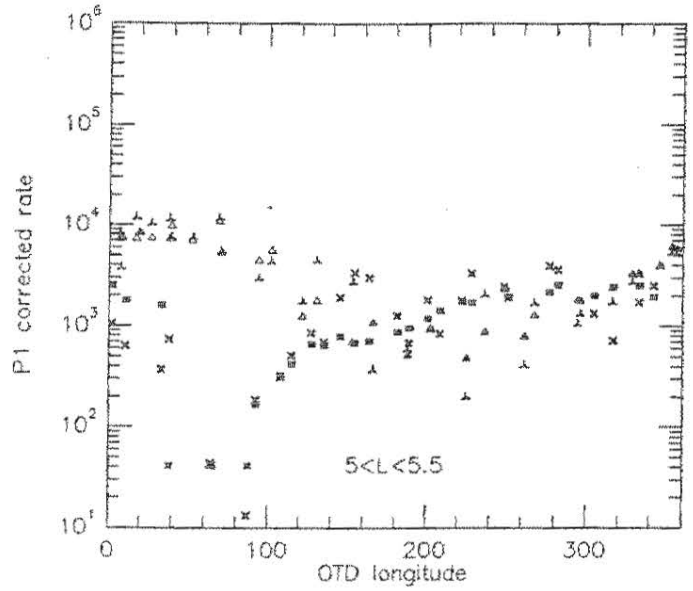
P1 corrected rate
OTD longitude
5<L<5.5

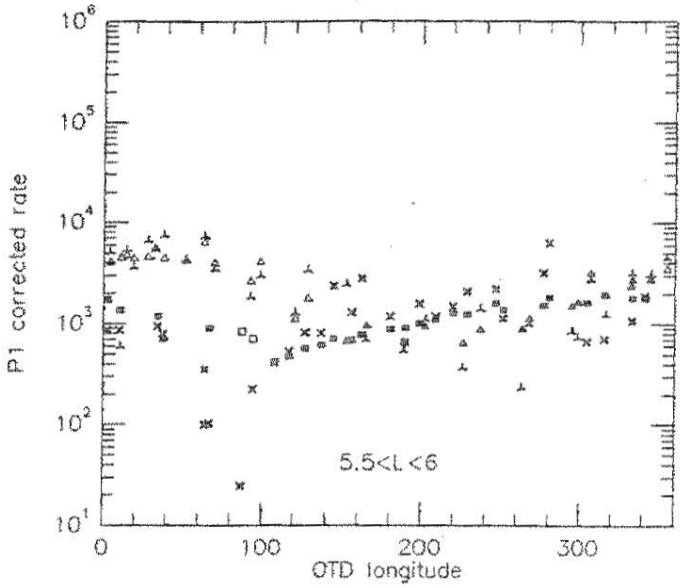
P1 corrected rate
OTD longitude
5.5<L<6

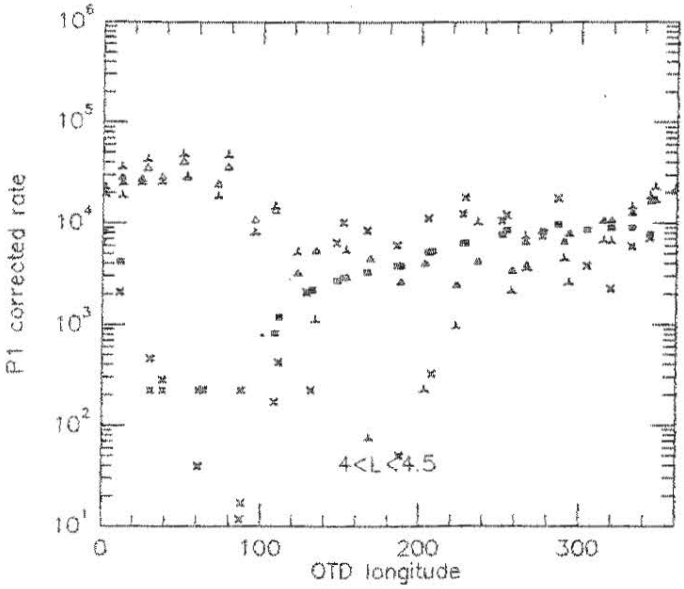
P1 corrected rate
OTD longitude
4<L<4.5

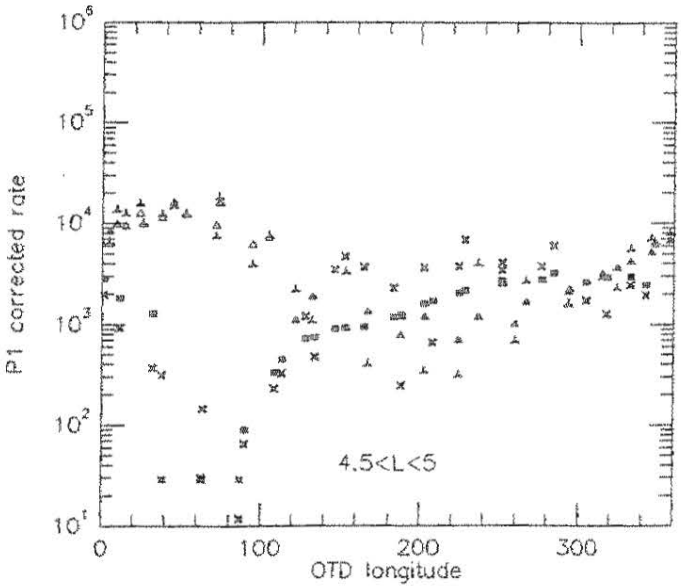
P1 corrected rate
OTD longitude
4.5<L<5

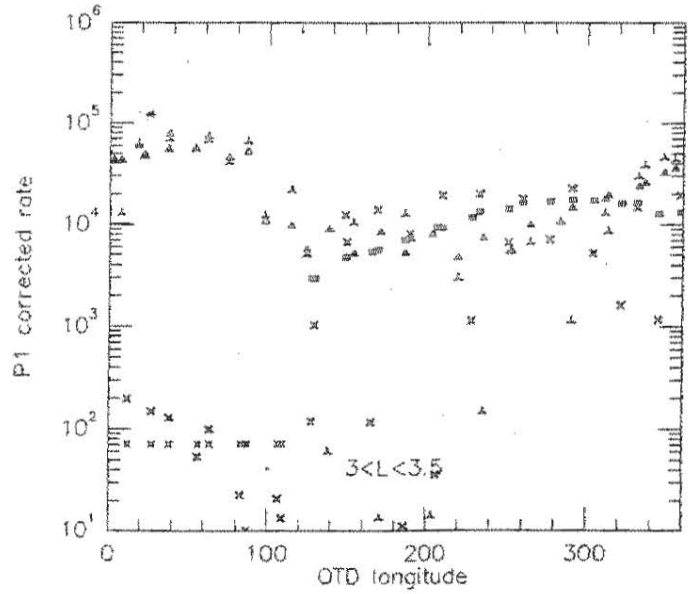
P1 corrected rate
OTD longitude
3<L<3.5

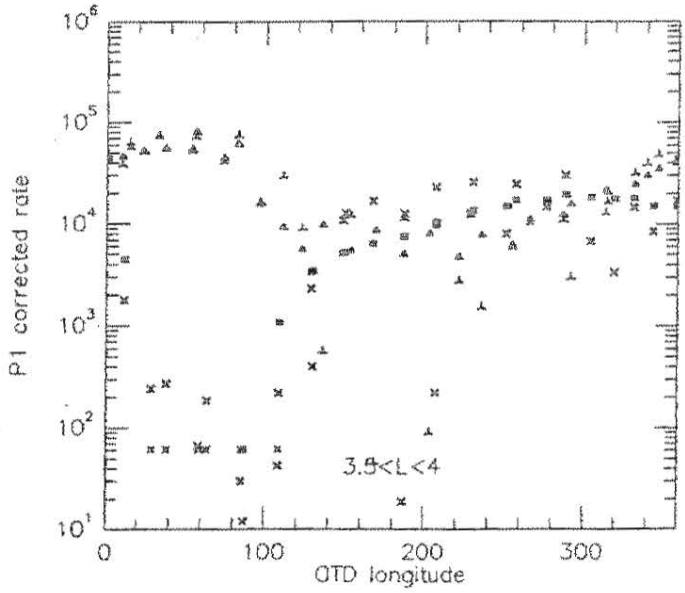
P1 corrected rate
OTD longitude
3.5<L<4

93/3

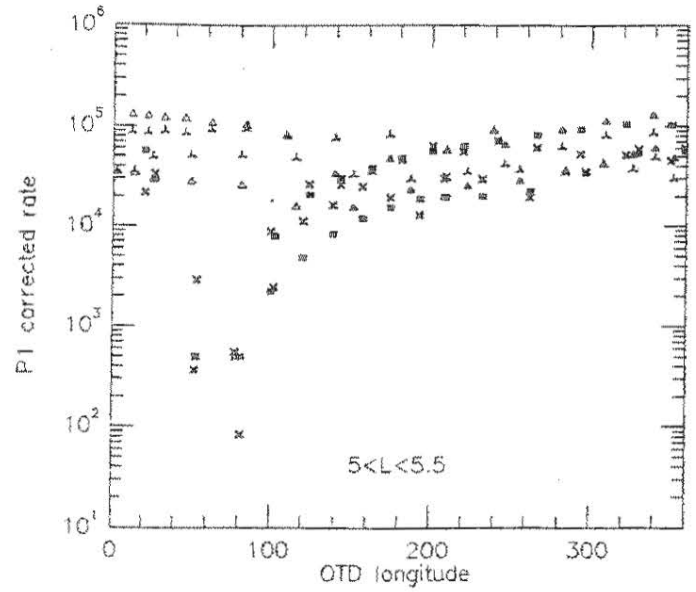
P1 corrected rate
OTD longitude
5<L<5.5

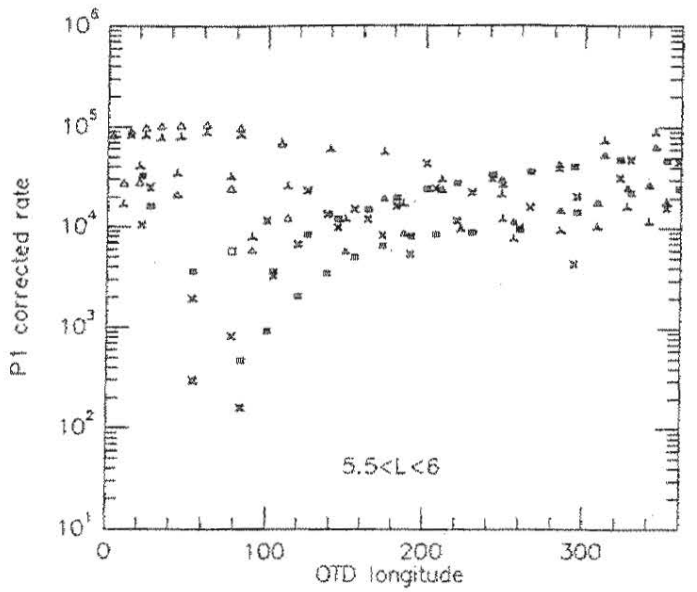
P1 corrected rate
OTD longitude
5.5<L<6

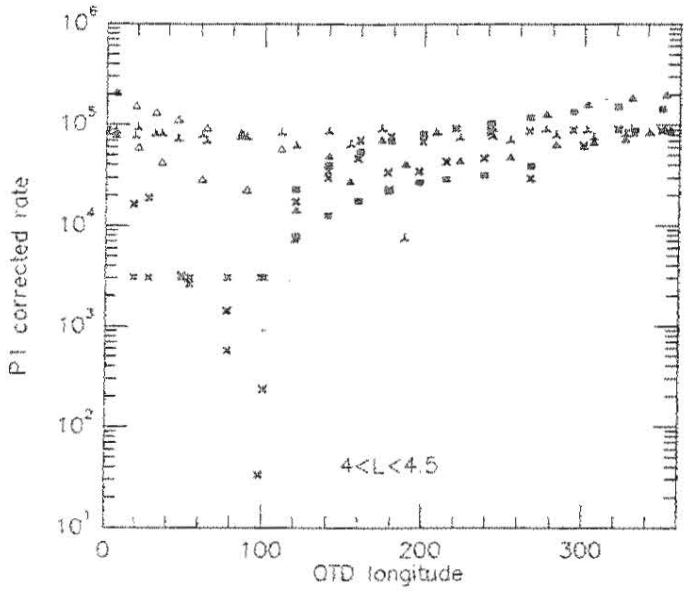
P1 corrected rate
OTD longitude
4<L<4.5

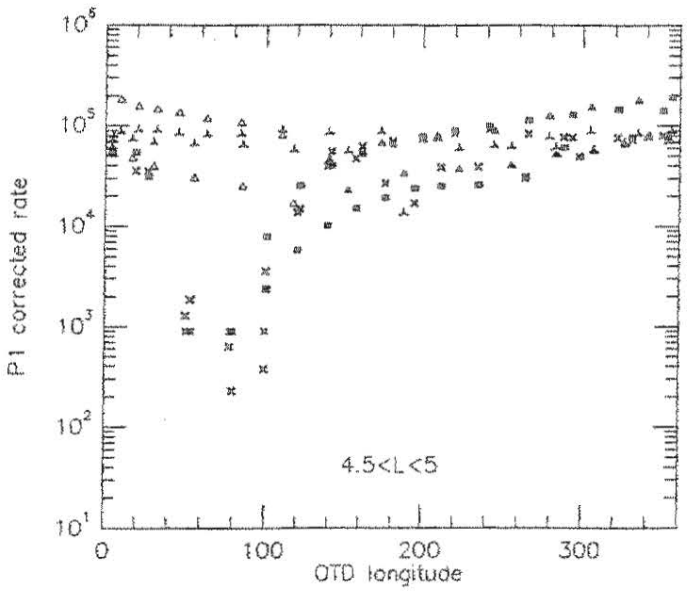
P1 corrected rate
OTD longitude
4.5<L<5

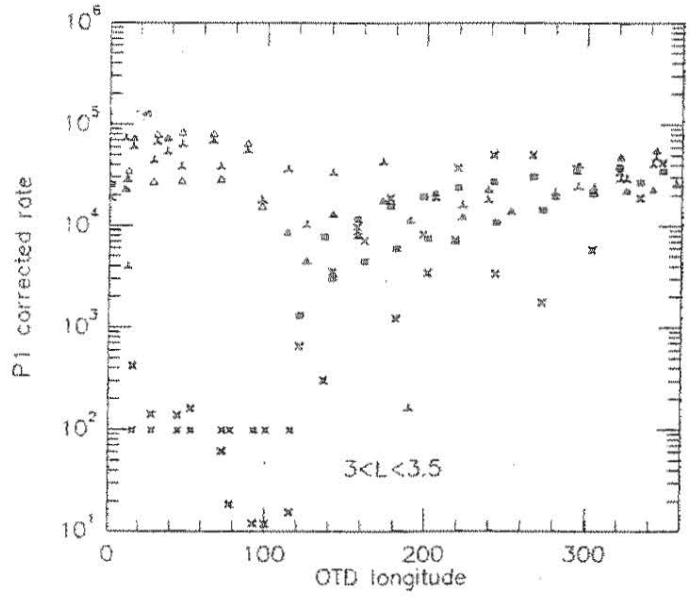
P1 corrected rate
OTD longitude
3<L<3.5

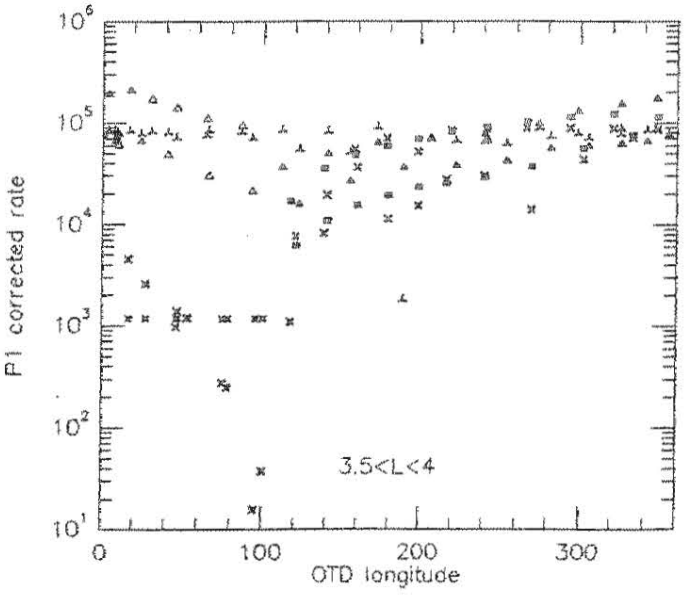
P1 corrected rate
OTD longitude
3.5<L<4

93/515

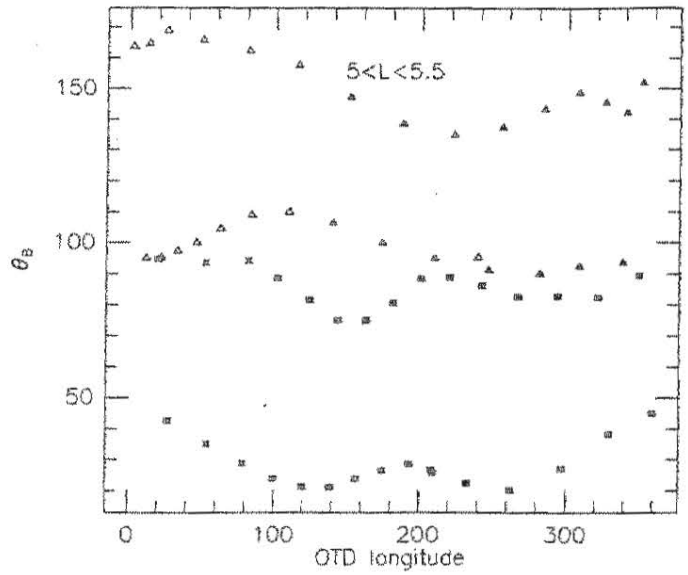
5<L<5.5
150
100
50
θ_B
0
100
200
300
OTD longitude

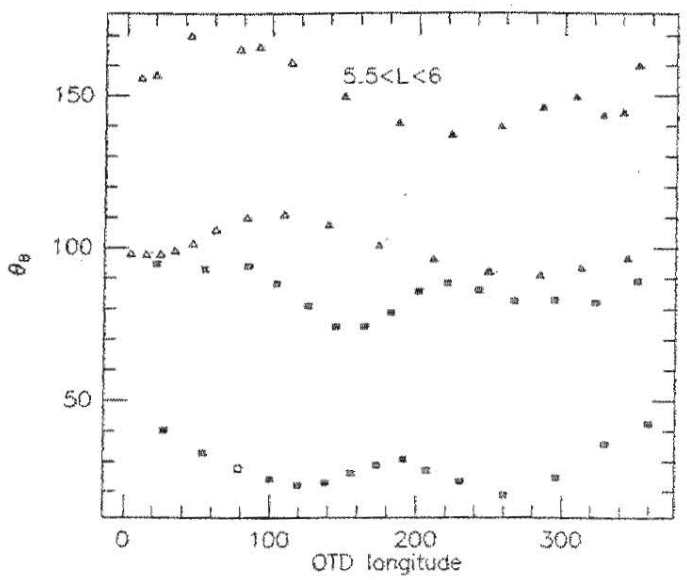
5.5<L<6
150
100
50
θ_B
0
100
200
300
OTD longitude

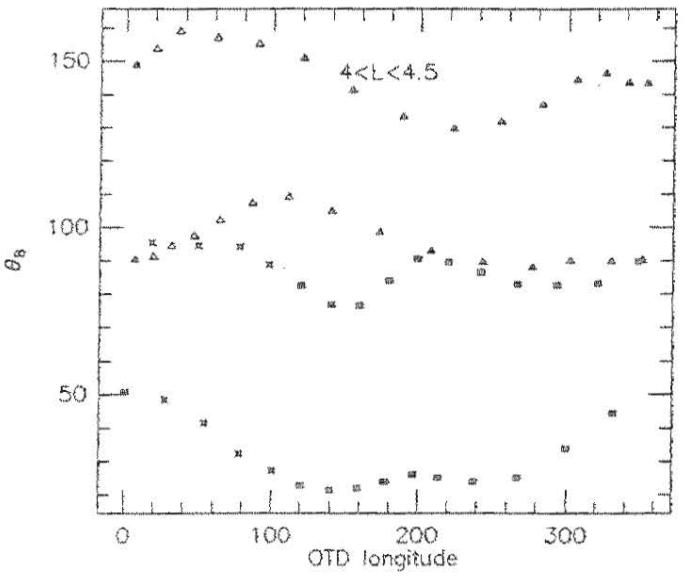
4<L<4.5
150
100
50
θ_B
0
100
200
300
OTD longitude

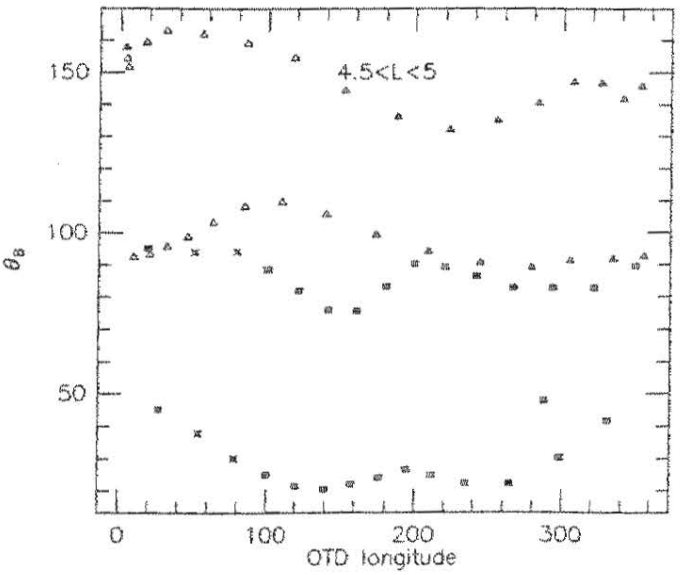
4.5<L<5
150
100
50
θ_B
0
100
200
300
OTD longitude

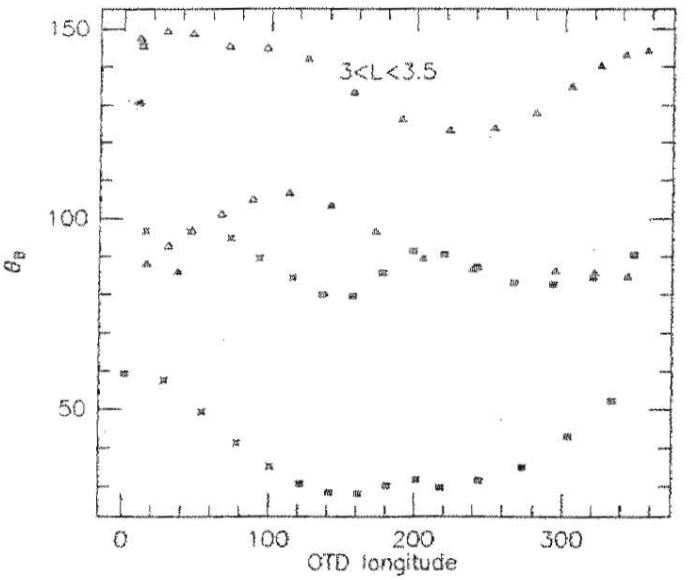
3<L<3.5
150
100
50
θ_B
0
100
200
300
OTD longitude

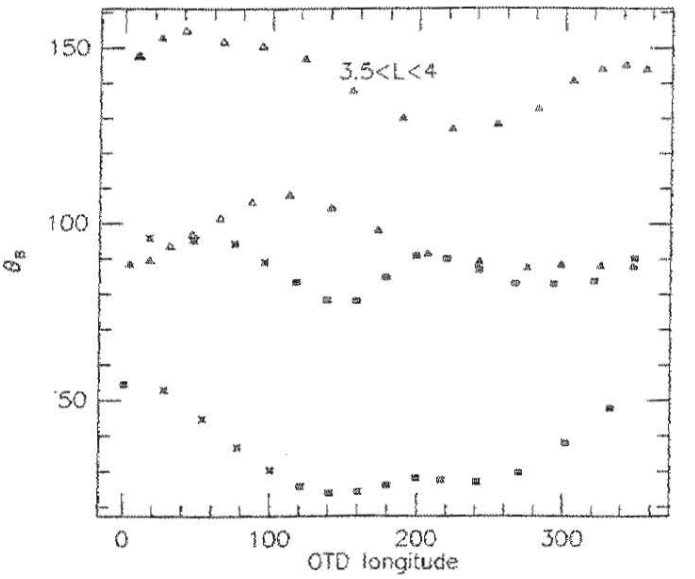
3.5<L<4
150
100
50
θ_B
0
100
200
300
OTD longitude

9 : 35

$\theta_B < 60$ or > 12

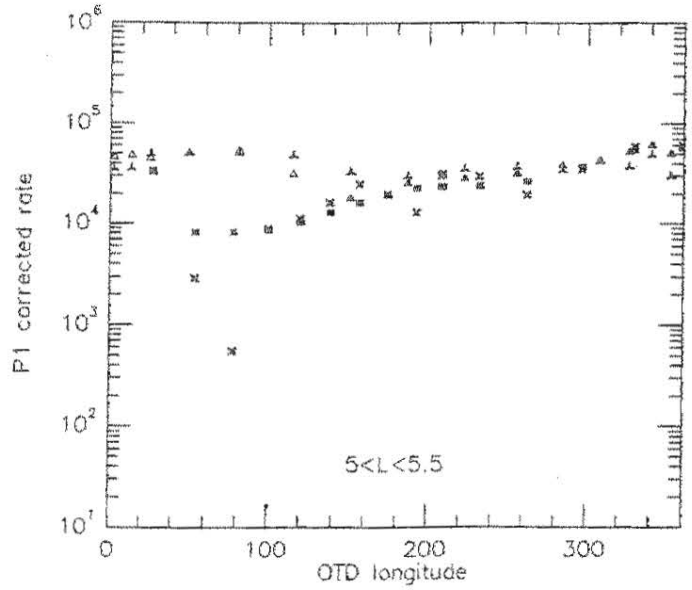

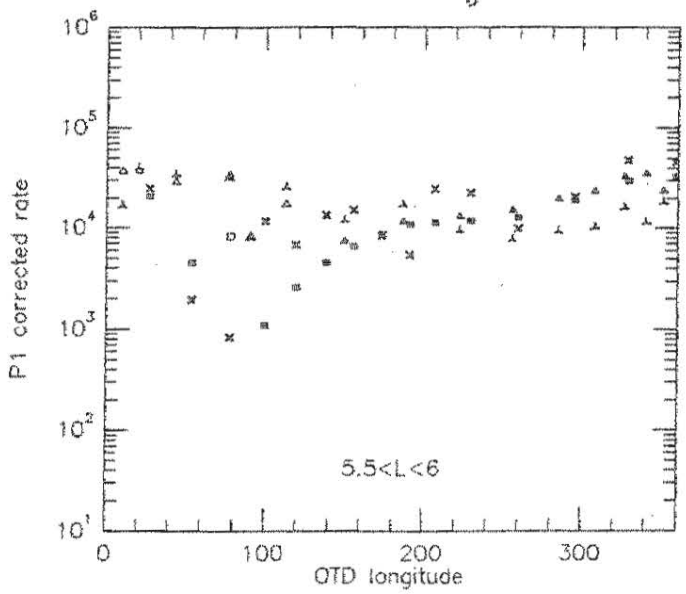

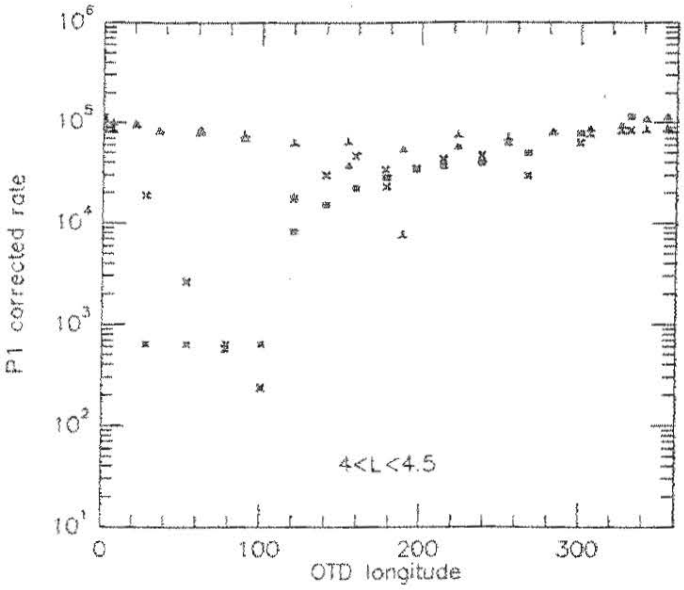

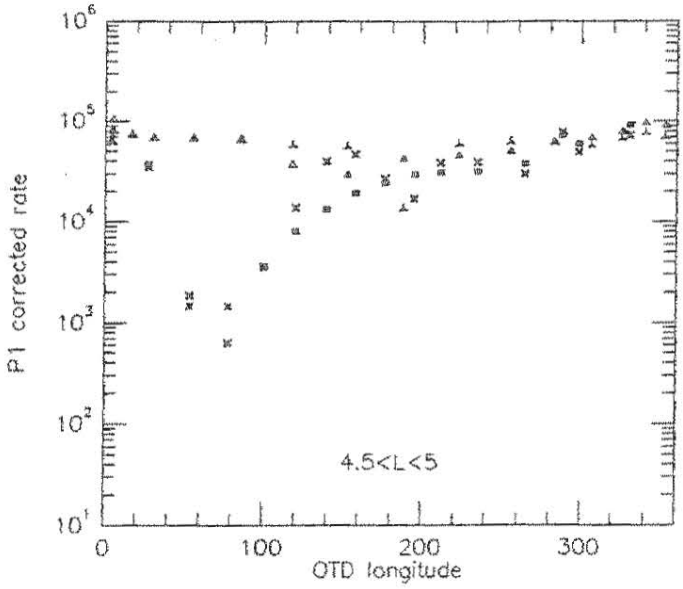

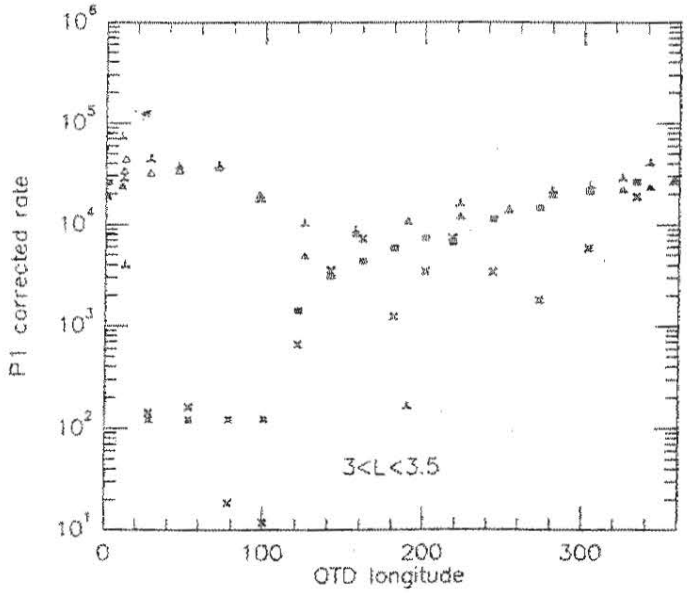

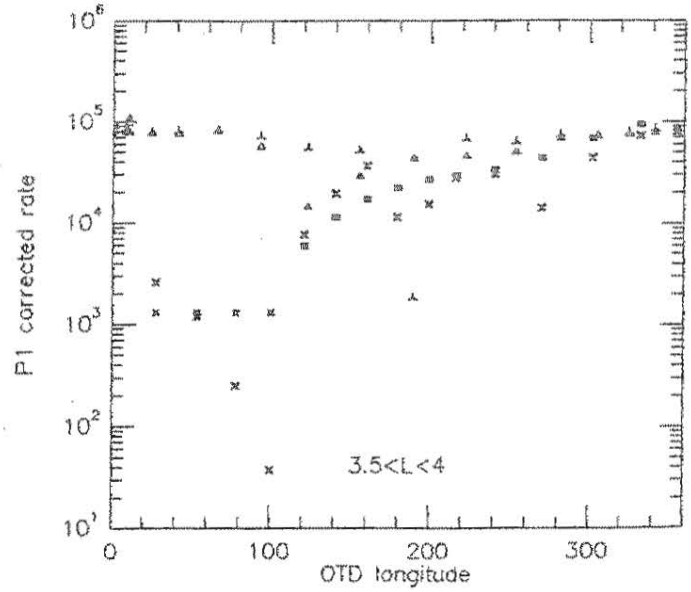

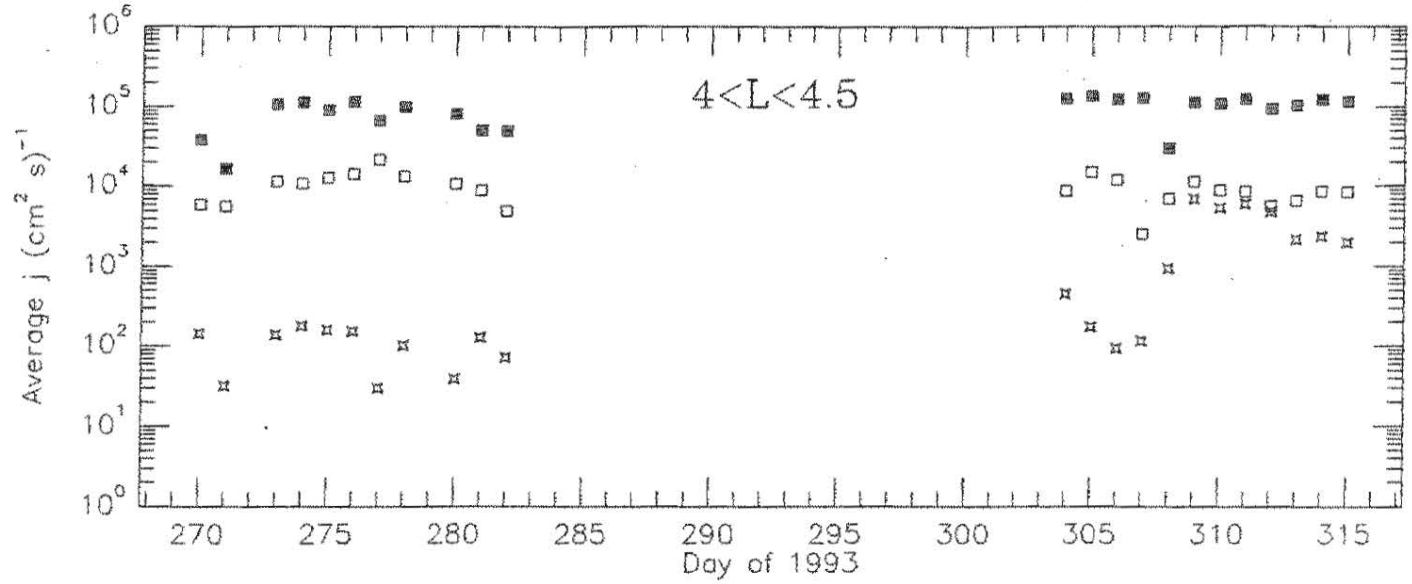
4<L<4.5
Average j (cm² s)⁻¹
Day of 1993

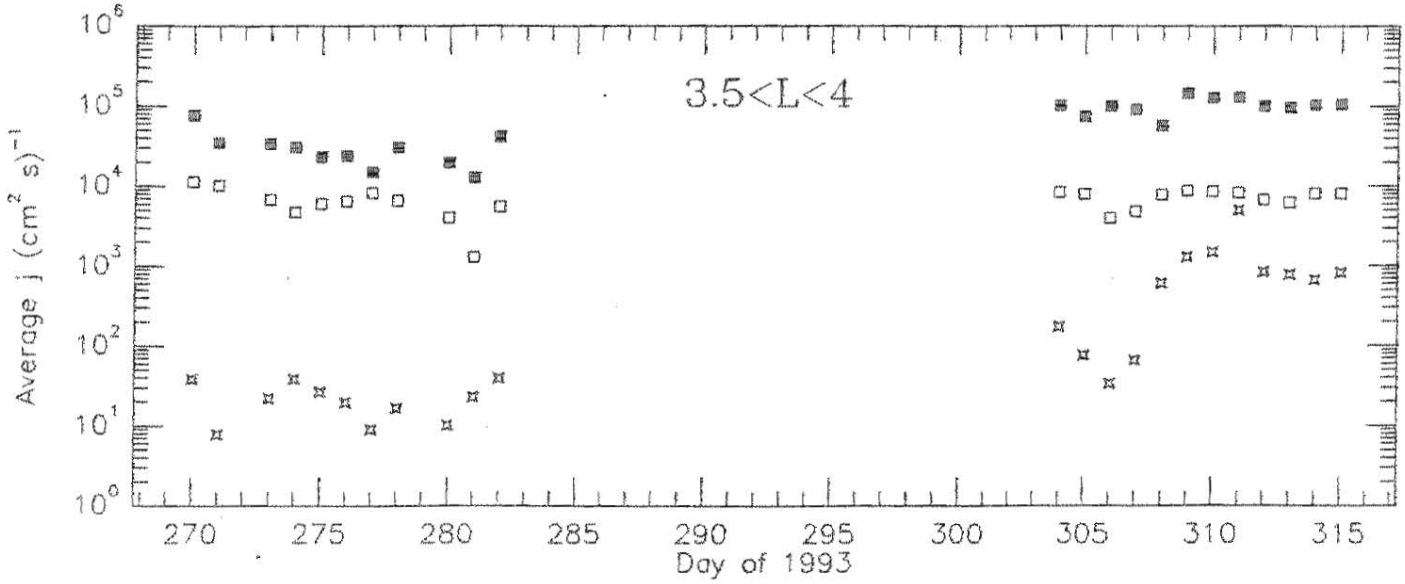
3.5<L<4
Average j (cm² s)⁻¹
Day of 1993

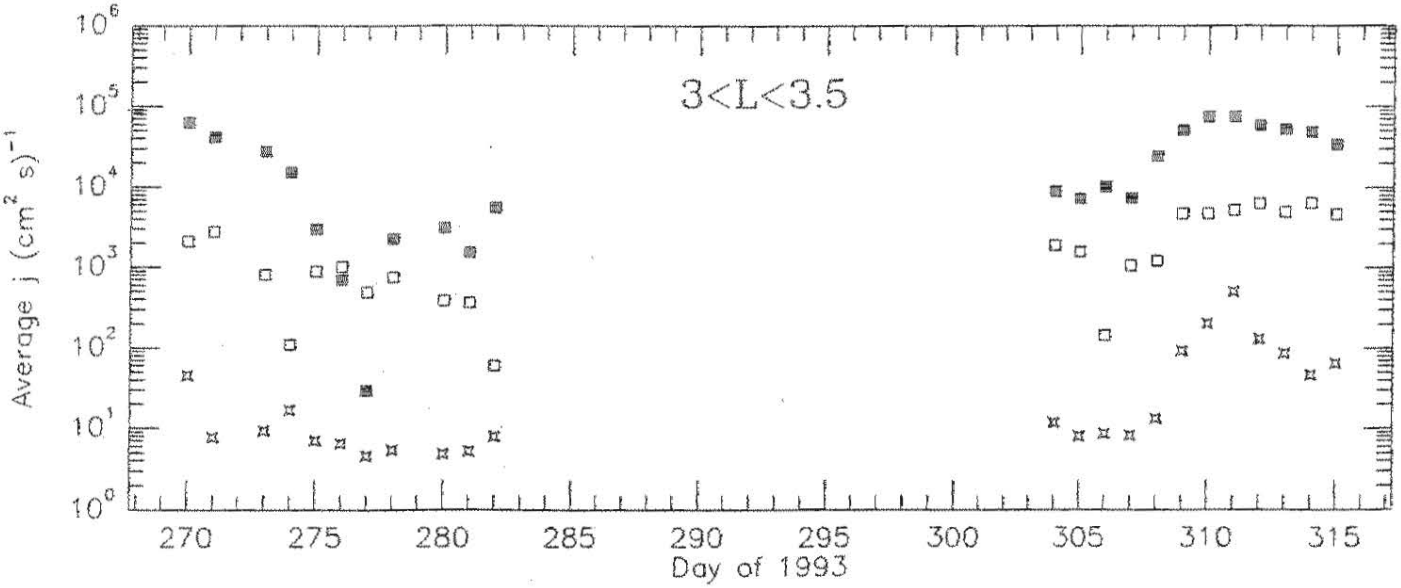
3<L<3.5
Average j (cm² s)⁻¹
Day of 1993

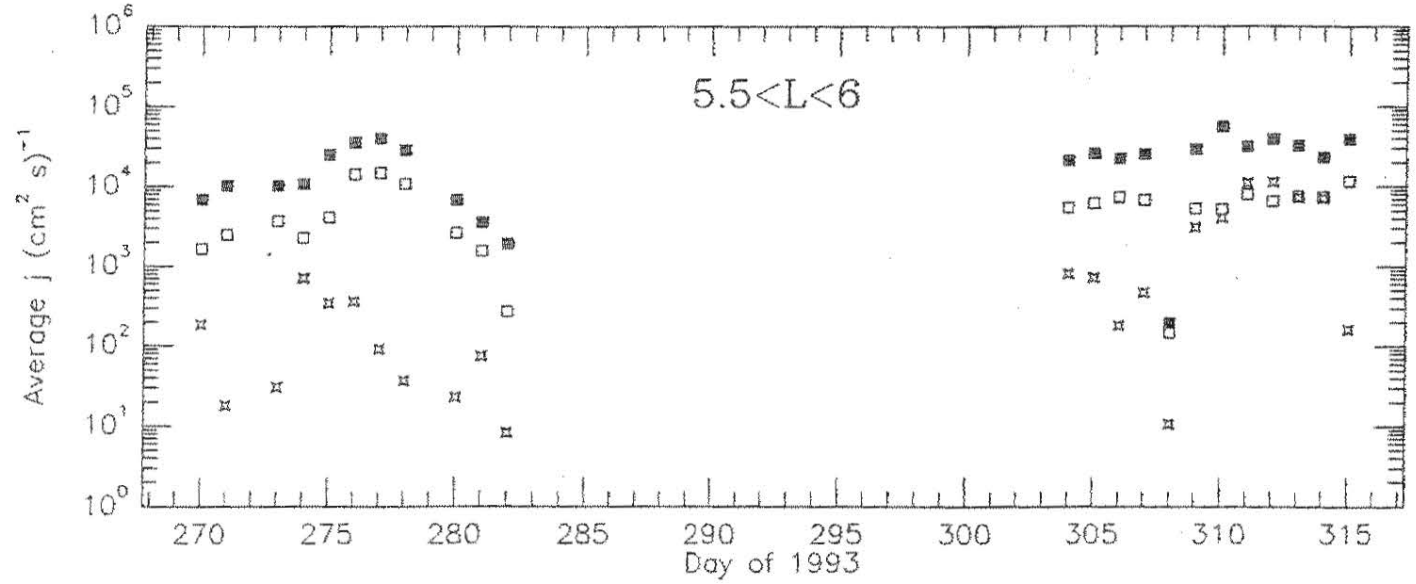
5.5<L<6
Average j (cm^2 s)$^{-1}$
10^6
10^5
10^4
10^3
10^2
10^1
10^0
270 275 280 285 290 295 300 305 310 315
Day of 1993

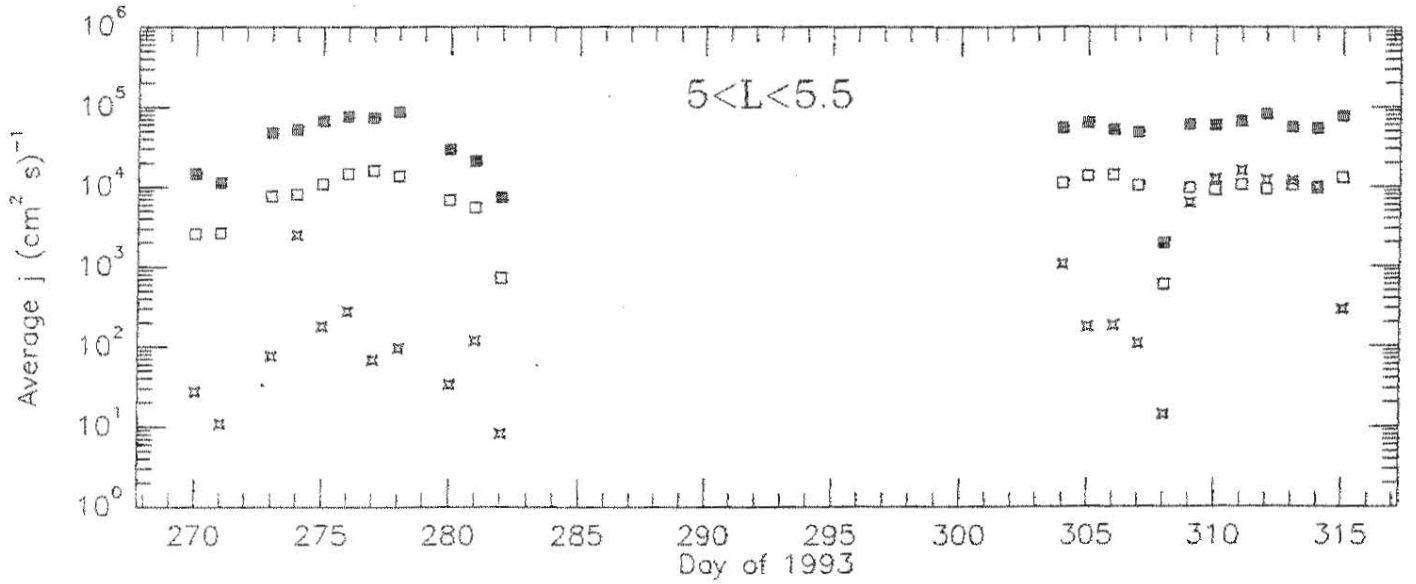
5<L<5.5
Average j (cm^2 s)$^{-1}$
10^6
10^5
10^4
10^3
10^2
10^1
10^0
270 275 280 285 290 295 300 305 310 315
Day of 1993

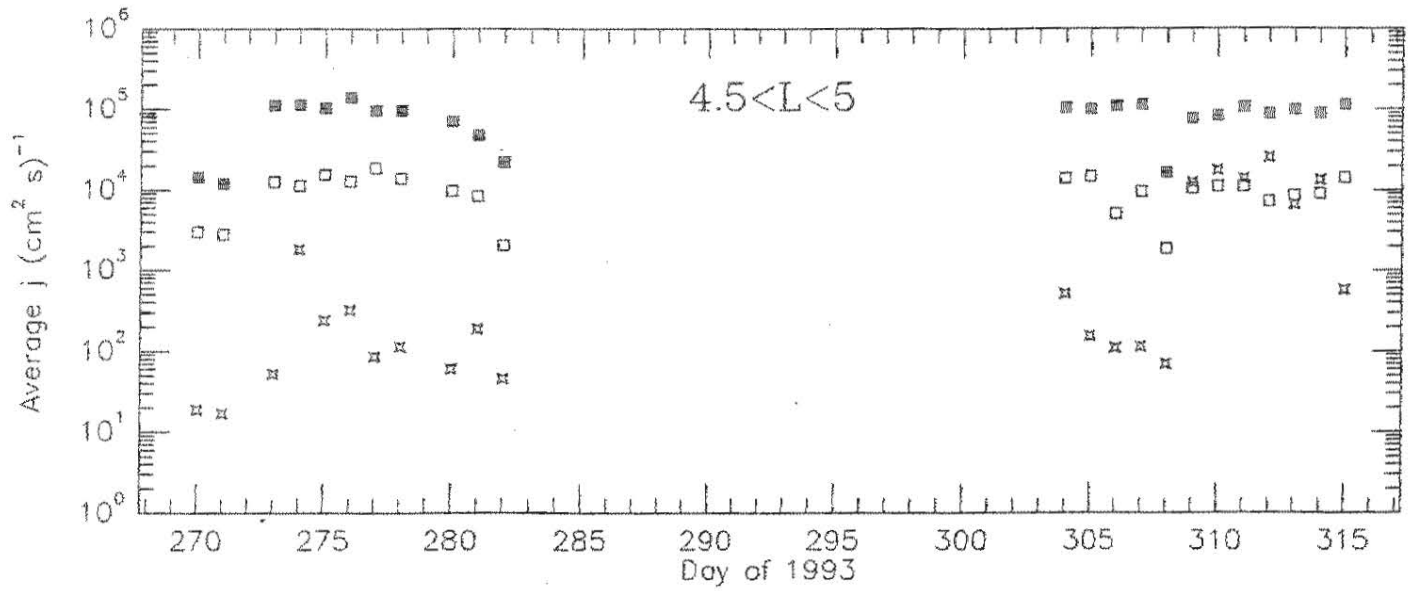
4.5<L<5
Average j (cm^2 s)$^{-1}$
10^6
10^5
10^4
10^3
10^2
10^1
10^0
270 275 280 285 290 295 300 305 310 315
Day of 1993

93/313

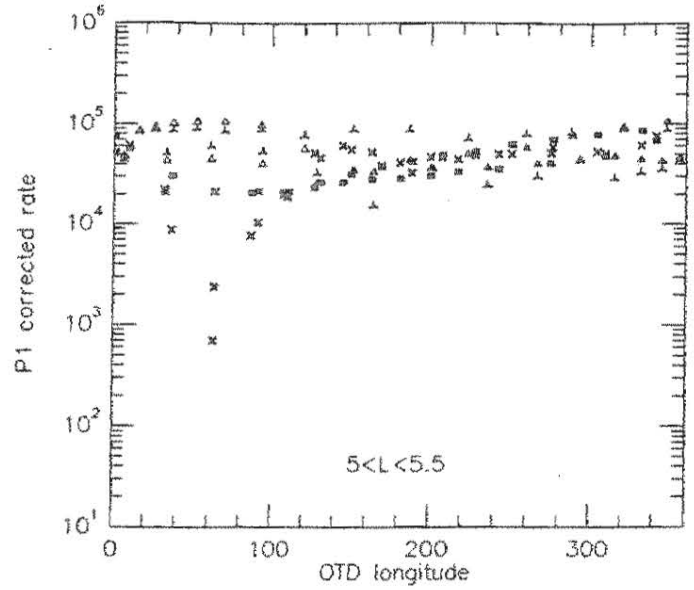
P1 corrected rate
OTD longitude
5<L<5.5

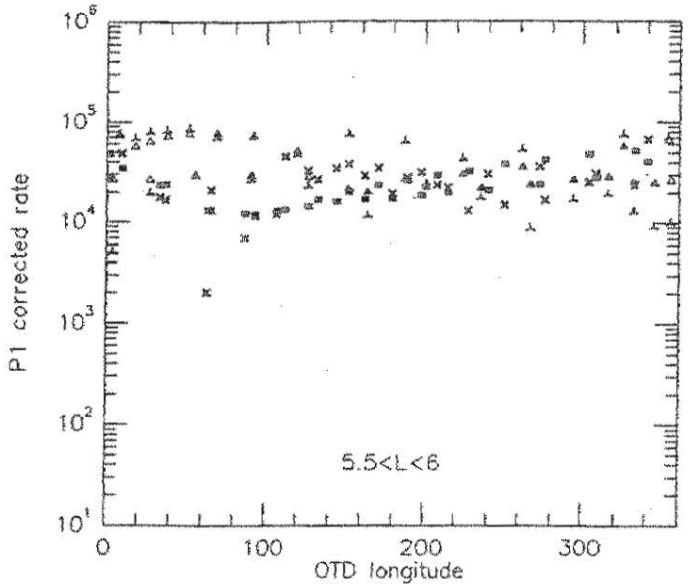
P1 corrected rate
OTD longitude
5.5<L<6

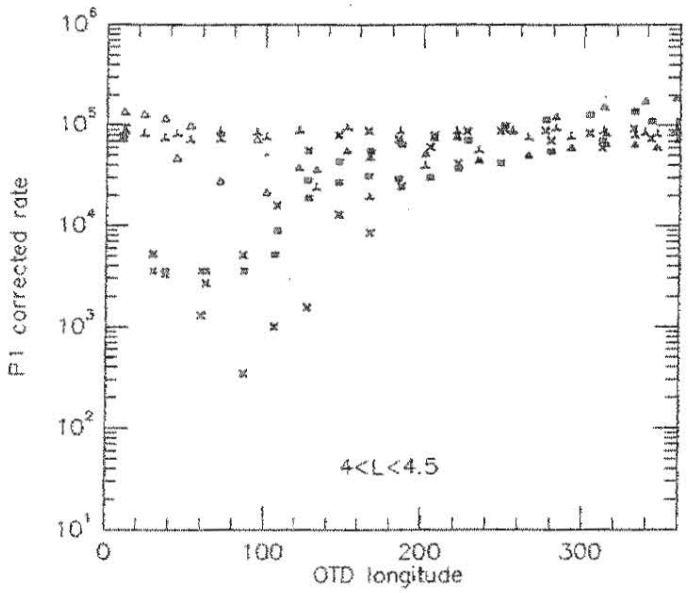
P1 corrected rate
OTD longitude
4<L<4.5

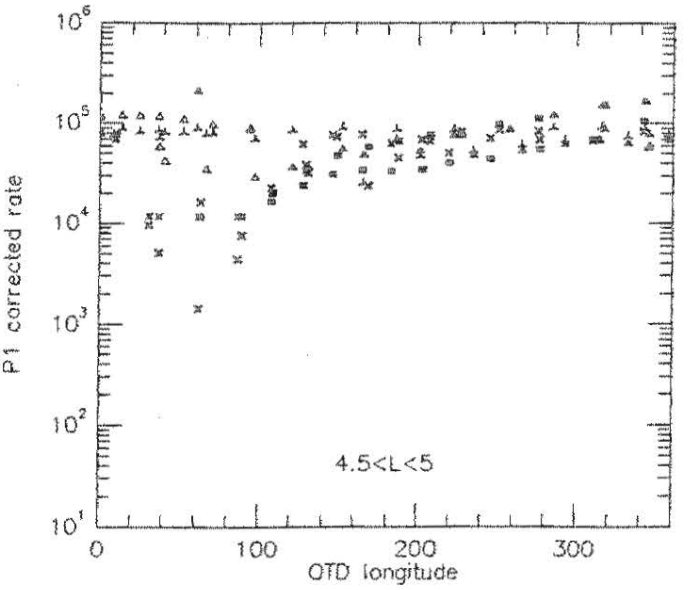
P1 corrected rate
OTD longitude
4.5<L<5

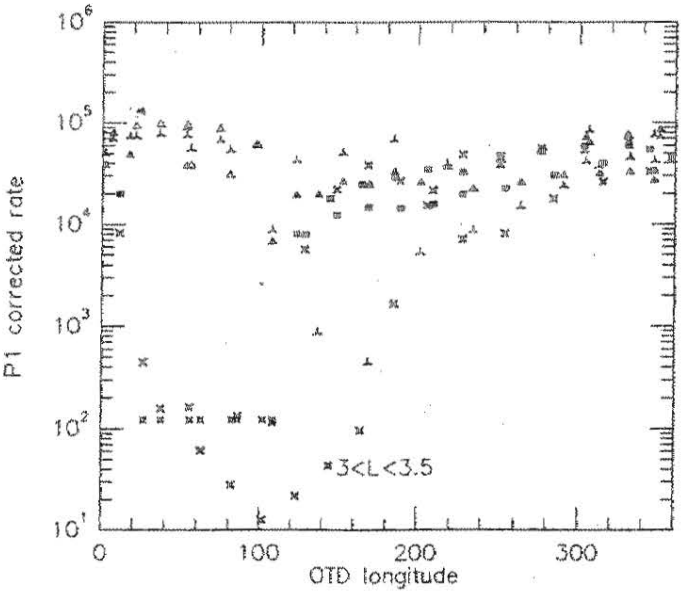
P1 corrected rate
OTD longitude
3<L<3.5

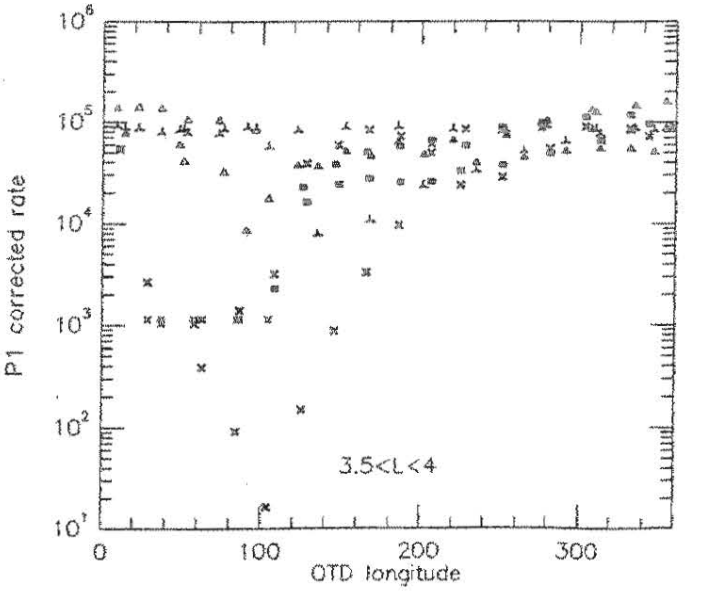
P1 corrected rate
OTD longitude
3.5<L<4